Chemical Physics 377 (2010) 109–114

Contents lists available at ScienceDirect

Chemical Physics

journal homepage: www.elsevier.com/locate/chemphys

YNi and its hydrides: Phase stabilities, electronic structures and chemical bonding properties from first principles

S.F. Matar [a,*], M. Nakhl [b], A.F. Al Alam [c], N. Ouaini [c], B. Chevalier [a]

[a] CNRS, Université de Bordeaux, ICMCB, 87 avenue du Docteur Albert Schweitzer, F-33608 Pessac, France
[b] Université Libanaise, Laboratoire de Chimie-Physique des Matériaux LCPM, Fanar, Lebanon
[c] Université Saint-Esprit de Kaslik, Faculté des Sciences et de Génie Informatique, Jounieh, Lebanon

ARTICLE INFO

Article history:
Received 4 May 2010
In final form 30 August 2010
Available online 20 September 2010

Keywords:
DFT
FeB-type
CrB-type
GGA
VASP
ASW
Hydrides
Equation of state
Chemical bonding

ABSTRACT

Within density functional theory, establishing the equations of states of YNi in two different controversial structures in the literature, leads to determine the orthorhombic FeB-type as the ground state one with small energy difference. For $YNiH_3$ and $YNiH_4$ hydrides crystallizing in the orthorhombic CrB-type structure the geometry optimization and the ab initio determination of the H atomic positions show that the stability of hydrogen decreases from the tri- to the tetra- hydride. New states brought by hydrogen within the valence band lead to its broadening and to enhanced localization of metal density of states. The chemical bonding analysis shows a preferential Ni–H bonding versus Y–H.

1. Introduction

Nickel based binary intermetallics are a relevant class of materials for a diversity of physical properties such as shape memory (e.g. TiNi) [1], *INVAR* magnetic alloys (e.g. Fe–Ni) [2] and intermetallics for hydrogen storage (e.g. CeNi) [3]. The search for compounds with large hydrogen density is important in the context of energy storage. For instance, YNi and ZrNi absorb up to 3 H per formula unit (fu) [4]. However recent reports on YNi and other *RE*Ni (*RE* is a rare earth) intermetallics indicate a higher absorption amount of ~4 H per fu [5], leading to ~3 wt.% hydrogen. This is similar to Mg_2NiH_4 which is characterized by ~3.6 wt.% hydrogen and reversible hydrogen adsorption ability [6].

On the other hand, the structural characterization of YNi has been controversial as far as early works by Smith and Hansen [7] report a monoclinic symmetry ($P2_1/b$ space group, SG) which is in disagreement with the study undertaken by Klepp and Parthé later on [8]. The latter found an orthorhombic *Pnma* symmetry with FeB-type structure. This primitive (P) orthorhombic type structure is less common in intermetallics because several *RE*Ni (*RE* = Ce, Sm, Gd) crystallize, like the corresponding tri- and tetra-hydrides, in the CrB-type structure (*Cmcm* SG) [5]. Nevertheless, it needs to be mentioned that the mecanosynthesis method of intermetallics and their hydrides using energetic ball milling, is known to induce some amorphisation and to produce different crystal structures than usual high temperature methods [9]. The ground state properties of intermetallics and the effects of hydrogen insertion such as the changes of the electronic structure and both the strength and character of the chemical bonding are important to understand at both the fundamental and applied levels. This is herein modeled within the well established quantum mechanical density functional theory (DFT) framework [10,11]. Firstly a search of the ground state structure of YNi is done in view of the controversy on its crystal structure, through calculating the respective equation of states (EOS) for monoclinic [7] and FeB-type [8] as well as CrB-type of the hydrides. Then the tri- and tetra-hydrides are examined with an ab initio determination of the atomic positions, mainly for H, in order to examine the relative stability of H within the intermetallic matrix [12].

2. Computational framework

Within DFT, calculations are performed using two complementary approaches. With pseudo-potential (PP) methodology, a geometry optimization of the lattice parameters is firstly carried out. Then the equilibrium energies and volumes are obtained through establishing the relevant energy/volume equations of

* Corresponding author.
E-mail address: matar@icmcb-bordeaux.cnrs.fr (S.F. Matar).

0301-0104/$ - see front matter © 2010 Elsevier B.V. All rights reserved.
doi:10.1016/j.chemphys.2010.08.022

state (EOS), as well as the relative binding energy of H within. This consists basically of PP's and plane waves coupled with a Fourier transform technique. The method implemented in different calculation methods, is used here within the VASP code [13]. It is extremely accurate and reasonably fast for materials modeling and especially it has shown good ability in predicting ground state structures [14]. A general characteristic, common to all the PP methods, is that once the description of the electronic interactions has been achieved, the forces acting on atoms can be easily calculated, thus giving the possibility to determine the minimum energy position for atoms belonging to the unit cell. Note that carrying out such calculations with all electrons methods would be much heavier and time consuming; unless massively parallelized computers are used.

VASP uses PP built both within the local density approximation (LDA) [15] and the generalized gradient approximation (GGA) [16] schemes for treating the exchange correlation XC effects. These are based on electron gas distribution which is close to that present in metals and alloys, like our case studies here. Typically, while the LDA underestimates lattice spacing, the GGA slightly overestimates it. However the use of one or the other XC functional is case sensitive and preliminary computations are carried out. When strongly correlated electrons system such as transition metal oxides are examined, electron gas based correlation needs to be enhanced by addition of an onsite repulsive parameter U [17]. The optimization of the structural parameters is performed until the forces on the atoms are less than 0.02 eV/Å and all stress components are less than 0.003 eV/Å^3. Computations are converged at an energy cut-off of 269.56 eV for the plane-wave basis set. The tetrahedron method with Blöchl corrections [18,19] as well as a Methfessel–Paxton scheme [20] for conducting systems are applied for both geometry relaxation and total energy calculations. Brillouin zone (BZ) integrals are approximated using a k-point sampling with a starting mesh of $4 \times 4 \times 4$ up to $8 \times 8 \times 8$ for best convergence and relaxation to zero strains. From the calculations the analysis of the charge density can assess the iono-covalent character change of hydrogen. The theoretical concept of atoms in molecules (AIM) introduced by Richard Bader [21], develops an intuitive way of dividing molecules into atoms as based purely on the electronic charge density. Bader uses what are called 'zero flux surfaces' to divide atoms. A zero flux surface is a 2-D surface on which the charge density is a minimum perpendicular to the surface. Typically in a chemical compound, the charge density reaches a minimum between atoms and this is a natural place to separate atoms from each other. Besides being an intuitive scheme for visualizing atoms in molecules, Bader's definition is often useful for charge analysis. For example, the charge enclosed within the Bader volume is a good approximation to the total electronic charge of an atom. Taking as an example the archetype metal hydride MgH_2, its high stability is translated by totally anionic hydrogen: H^{-1}. This hinders its use for application. The addition of Ni leading to Mg_2NiH_4 reduces the anionic character and H^{-1} becomes $H^{-0.8}$ as inferred from Bader charge analysis [14,21]. We shall show that such trends are observed in presently investigated hydrides.

Then all-electron calculations are needed to explore the electronic structure within the whole valence band (VB) and conduction band (CB) as well as details of the chemical bonding. This is performed using the scalar-relativistic ASW method [22,23]. The method uses the atomic sphere approximation ASA which assumes overlapping atomic spheres whose volume is equal to the cell volume. Likewise, the computations are based on DFT and the GGA scheme as parameterized by Wu and Cohen [24]. This scheme is preferred to LDA one (as well as in PP calculations), for better energy-volume quantities versus experiment in present case studies. In this method, the wave function is expanded in atom-centered augmented spherical waves, which are Hankel functions and numerical solutions of Schrödinger's equation, respectively, outside and inside the so-called augmentation spheres. In the minimal ASW basis set the outermost shells represent the valence states and the matrix elements are constructed using partial waves up to $l_{max} + 1 = 3$ for Y and Ni and $l_{max} + 1 = 2$ for H (l: secondary quantum number). Calculations are started for neutral atom configurations. Convergence is obtained when negligible variations for the charge densities ($\Delta Q = 10^{-8}$) and for the total energy ($\Delta E = 10^{-7}$ eV), are observed between two successive iterative cycles. Further the relatively open (low compactness) structure of the hydrides due to the expansion of the pristine YNi intermetallic, empty spheres (ES) are introduced within ASA. ES are pseudo atoms with zero atomic numbers and a limited valence basis set like hydrogen. They are introduced at interstitial lattice sites and they receive charges from neighboring atoms, thus allowing for a continued charge density within the lattice. The choice of the sites as well as the augmentation radii are automatically determined using the sphere-geometry optimization algorithm [25]. The BZ integrations are performed using Blöchl linear tetrahedron method with up to 576 k-points within the irreducible wedge [18].

In order to answer the basic question, "*where are the electrons*?", Roald Hoffmann introduced the COOP (crystal orbital overlap populations, in early extended-Hückel type calculations [26]. The COOP are calculated based on the overlap matrix elements $c^*_{ni}(\mathbf{k})S_{ij}c_{nj}(\mathbf{k}) = c^*_{ni}(\mathbf{k}) < \chi_{\mathbf{k}i}(\mathbf{r})|\chi_{\mathbf{k}j}(\mathbf{r}) > c_{nj}(\mathbf{k})$ where S_{ij} is an element of the overlap matrix formed of the valence basis functions, χ and $c_{nj}(\mathbf{k})$ are the expansion coefficients entering the expression of the wave function of the nth band. The partial COOP coefficients, $C_{ij}(E)$, are then obtained by integrating the above expression over the Brillouin zone (BZ): $C_{ij}(E) = C_{ji}(E) = 1/\Omega_{BZ}\sum_n \int_{BZ} d^3\mathbf{k}\, Re\{c^*_{ni}(\mathbf{k})S_{ij}c_{nj}(\mathbf{k})\}\delta(E - \varepsilon_{n\mathbf{k}})$; where Ω_{BZ} is the Brillouin zone volume, δ is the Dirac *delta* notation, serving as counter of states and *Re* refers to the real part of following expression. The total COOP, $C(E)$, are evaluated as a summation over the non diagonal elements: $C(E) = \sum_{ij(i\neq j)} C_{ji}(E)$. The COOP is implemented within ASW method as a reliable way for assessing the chemical bonding in a DFT based program [27]. It is used in present work as integrated COOP (*i*COOP). In the plots, positive, nil and negative COOP area magnitudes are indicative of bonding, anti-bonding, and non-bonding interactions, respectively. We also note that another scheme uses the Hamiltonian based populations with the COHP (crystal orbital Hamiltonian populations) [28]. It is described similarly to the COOP while replacing the overlap matrix by Hamiltonian one, H_{ij}. Lastly more recent developments led to use both approaches to propose the «covalent bond energy» criterion, ECOV [29]. A partial $ECOV_{ij}$ is then proportional to $COHP_{ij}(E) - COOP_{ij}(E)$.

3. Geometry optimization from pseudo-potential calculations

3.1. YNi

In view of the published controversial structures [7,8], we have revisited YNi to establish the ground state structure. Beside the monoclinic and the orthorhombic forms we also consider hypothetic CrB-type form, which is adopted by the hydrides. Using the crystal data from the literature [4,7,8] as starting values, geometry relaxation was carried out. In all three cases, monoclinic, orthorhombic FeB and CrB types, the lattice symmetry was preserved and the optimized cell volumes showed a good agreement with experiment for the monoclinic (calc. 160.7/exp. 160.4 Å^3) as well as the orthorhombic (calc. 160.5/exp. 162.7 Å^3) structures and a smaller value calculated for CrB-type YNi: 159 Å^3.

Examining the ground state FeB-type structure, we show in Table 1 the experimental and calculated lattice parameters. The calculated values show a good agreement with experiment. The

Table 1
Geometry optimization results as compared to experiment for YNi in FeB-type structure.

YNi *Pnma*	Experiment [8]	Calculated
a-latt. const. (Å)	7.156	7.054
b/a	0.576	0.556
c/a	0.771	0.768
Volume (Å^3)/4 fu	162.76	160.3
Y	0.1798, ¼, 0.1325	0.181, ¼, 0.133
Ni	0.0357, ¼, 0.6233	0.037, ¼, 0.626
Distances (Å)		
Y–Ni	2.897–2.913	2.85–2.93
Y–Y	3.587	3.56
Ni–Ni	2.522	2.56

shortest interatomic distance is observed between two Ni nearest neighbors, while Y–Y has the largest separation. These distance trends are also observed for the monoclinic form. It will be shown that the Y–Ni distance increases with the insertion of hydrogen (cf. Table 2).

In order to establish energy trends, the equation of state (EOS) is needed, i.e. one cannot rely solely on the quantities obtained from plain lattice optimizations, especially when comparisons of energies and of volumes magnitudes are to be done between different phases. The underlying physics is that the calculated total energy corresponds to the cohesion within the crystal; in as far as the solution of the Kohn–Sham DFT equations gives the energy with respect to infinitely separated electrons and nuclei. But the zero of energy depends on the choice of the pseudo-potentials, then energy becomes arbitrary through its shifting, not scaling. However the energy derivatives as well as the EOS remain unaltered. For this reason one needs to establish EOS's from which the fit parameters are extracted for an assessment of the equilibrium values. This can be done from a set of $E(V)$ calculations for all three forms of YNi. The resulting curves shown in Fig. 1 have a quadratic variation which can be fitted with Birch EOS to the 3rd order [30]:

$$E(V) = E_o(V_o) + [9/8]V_oB_o[([(V_o)/V])^{[2/3]} - 1]^2 + [9/16]B_o(B' - 4)V_o[([(V_o)/V])^{[2/3]} - 1]^3,$$

where E_o, V_o, B_o and B' are the equilibrium energy, the volume, the bulk modulus and its pressure derivative, respectively. While the B' value amounts to 4, a magnitude usually observed (Ref. [31] and

Table 2
Geometry optimization results for $YNiH_3$ and $YNiH_4$ in *Cmcm* SG. Starting H coordinates are from Peterson et al. [28]. Data for YNi in same hypothetic SG are added for comparison.

System	YNi	$YNiH_3$	$YNiH_4$
a-latt. const. (Å)	3.76	3.648	3.660
b/a	2.700	3.065	3.126
c/a	1.100	1.249	1.278
Volume (Å^3)/4 fu	158.63	185.24	196.04
Y, Ni and H1 at 4*c* (0, *y*, 1/4)			
y_Y	0.140	0.137	0.132
y_{Ni}	0.428	0.422	0.404
y_{H1}	–	0.929	0.914
H2 at 8*f* (0, *y*, *z*)	–		
y	–	0.316	0.307
z	–	0.503	0.504
H3 at 4*b* (0, ½, 0)	–	–	Idem
Distances (Å)			
Y–Ni	2.87	3.02	3.10
Y–H1	–	2.32	2.40
Y–H2	–	2.22	2.27
Y–H3	–		2.40
Ni–H1	–	1.83	1.83
Ni–H2	–	1.63	1.61
Ni–H3	–		1.62

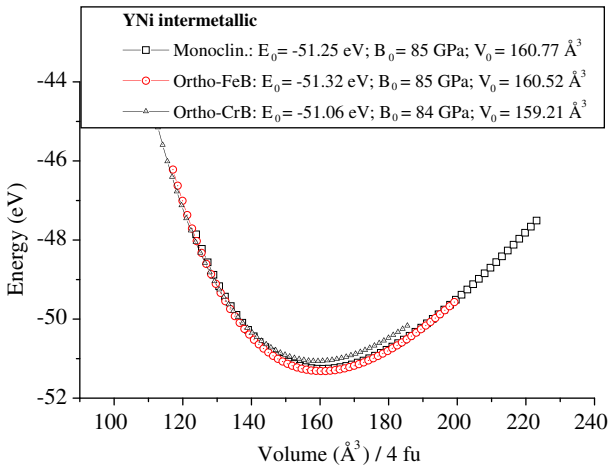

Fig. 1. Energy versus volume curves for three forms of YNi and fit results from Birch EOS showing the stabilization of the orthorhombic FeB-type structure.

therein cited works), the equilibrium fit values shown in the insert of Fig. 1 indicate magnitudes of volumes in agreement with experiment. There are slight differences with respect to geometry optimized values (Tables 1 and 2) due to the two different methods of obtaining them, i.e. energy minimization with geometry optimization versus energy derivatives with EOS. The values of total energies are close but, in as far as all calculations were carried out in the same convergence conditions, it is shown that the ground state is for FeB-type YNi with −0.08 eV stabilization with respect to monoclinic phase, while the hypothetic CrB-type adopted by the hydrides is clearly destabilized with respect to the monoclinic phase by 0.19 eV. The close total energies of the two experimental structures indicate that they can both be stabilized. A transformation may occur by energetic ball milling [9] for instance. In all three phases the bulk modulus B_0 amounts to ~85 GPa, a value usually found for intermetallics such as CeNi [31].

3.2. $YNiH_3$ and $YNiH_4$

The $YNiH_3$ [3] and $YNiH_4$ [5] hydrides crystallize in the base centered orthorhombic *Cmcm* space group with CrB-type structure. There are four formula units (fu) per cell, but due to the base centered C-centering SG, only two fu are explicitly accounted for in the calculations. The uptake of 3 hydrogen atoms per fu, results in an isotropic expansion of the cell and hydrogen atoms are dispatched over two different sets of sites. Within the *Cmcm* SG, H1, Y and Ni are, in Wyckoff notation, at 4*c* positions and H2's are at 8*f*. H1 and H2 are then found in Y_3Ni_2 trigonal bipyramids and Y_3Ni tetrahedra, respectively. This is depicted in Fig. 2. When extra hydrogen (H3) is inserted, Yaropolov et al. [5] suggest the 4*b* (0, ½, 0) position shown as black squares in Fig. 2. In as far as no data are available for the general positions; we started from the crystal data of Peterson et al. [32] for isopointal $ZrNiH_3$.

After geometry optimization the orthorhombic symmetry is kept for both hydrides within *Cmcm* SG; also hypothetic *Cmcm*-YNi was calculated to enable comparisons. The calculated values of lattice parameters and internal atomic coordinates are given in Table 2. In the hydrides the main effect of increasing H content upon going from the tri- to the tetra-hydride, is the increase of Y–H separation while the Ni–H distances remain almost unchanged. These trends in metal-hydrogen distances are similar to those of formerly studied $ZrNiH_3$ [33], i.e. d(Zr(Y)–H) > d(Ni–H). This should be exhibited by the chemical bonding between Y(Ni) and hydrogen discussed below. Furthermore, the volume calculated for $YNiH_4$, $V = 196$ Å^3 is close to the experimental value: $V_{exp.} \sim 200$ Å^3 [5].

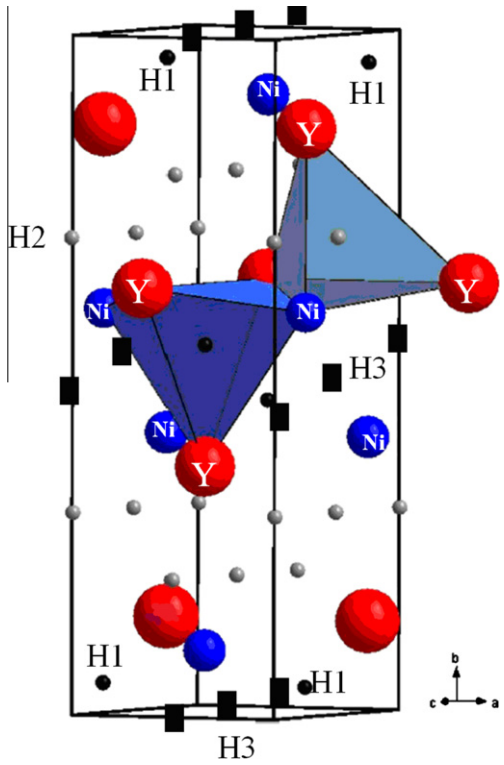

Fig. 2. Sketch of the $YNiH_3$ and $YNiH_4$ hydrides and coordination polyhedra for H1 and H2 in $YNiH_3$; additional 'H3' (black square) leads to the tetra-hydride.

From the energy results we examine the stability of hydrogen within the hydride systems using the following expression:

$$E_{\text{bind.}} = E_{(\text{YNiHX})} - E_{(\text{YNi})} - x/2E_{(\text{H2})}; x = 3 \text{ and } 4.$$

While the two first terms of the right-hand-side equality are the energy values obtained from the calculations, $E(H_2)$ is derived from pseudo-potential calculations of dihydrogen. The resulting energy amounts to −6.595 eV. With above equation we extract the stabilization energy of hydrogen in the hydride lattice: $E_{\text{H-bind.(YNiH3)}} = -1.915$ eV and $E_{\text{H-bind.(YNiH4)}} = -2.238$ eV, i.e. resp. −0.64 and −0.56 eV per H. Although indicating stabilized hydrogen within YNi, these values are of smaller magnitude compared to similarly calculated H stabilization within $ZrNiH_3$ which amounts to ∼−1 eV [33]. Further when the amount of H increases from the tri- to the tetra-hydride, hydrogen is found less bonded to the metal lattice. This allows suggesting that the departure of H from $YNiH_4$ then $YNiH_3$, is easier than in the Zr homologue.

These results are further quantified from the charge density analysis within AIM theory presented above. Taking MgH_2 as a reference, the charge on H is −1. In $YNiH_3$ we compute H charge ranges from −0.8 to −0.6. For $YNiH_4$, beside these charges characterizing H1 and H2 the additional hydrogen H3 carries a −0.3 charge, making it behave as the most covalent among the hydrogen belonging to the three sites. Then, additional H3 at 4*b* (0, ½, 0) should be the first hydrogen to be desorbed. This illustrates the destabilization of the tetra-hydride with respect to the tri-hydride.

4. All electrons calculations

Using the geometry optimized structural data (cf. Table 1); calculations of the electronic structure and properties of chemical bonding were then carried out for YNi and its hydrides $YNiH_3$ and $YNiH_4$. YNi is considered in the CrB-type structure adopted by the hydrides to enable comparisons with these H-based systems. Preliminary densities of states (DOS) calculations in FeB-type structure show the same features.

At energy self-consistent convergence a slight charge transfer exchange (∼0.3 electrons) is observed from Y toward Ni within YNi and from Y to Ni and H in the hydrides as well as to the ES with much lower amounts, i.e. they receive charge residues from neighboring atoms. This is concomitant with the electronegativity order of these species at the Pauling scale [34], i.e. the less electronegative Y ($\chi = 1.2$) gives away charges to more electronegative Ni ($\chi = 1.9$) and H ($\chi = 2.2$). However these transfers are not meaningful of an ionic character which is not encountered in such calculations; it can be rather argued that the quantum mixing between the valence states will show the major character of interaction between the atomic constituents of such an intermetallic hydride.

4.1. Density of states

The site projected densities of states (PDOS) are shown in Fig. 3 for YNi and its hydrides, respectively. In these plots as well as in following ones, energy reference is taken with respect to the Fermi level E_F. Furthermore, the same energy window, i.e. from −12 to 6 eV, is considered for the PDOS of these three systems crystallizing within the same SG (*Cmcm*). For YNi (Fig. 3a), the valence band (VB) is mainly dominated by Ni d states centered below E_F. This is due to Ni being a late element in the 3d series, i.e. having its d subshell populated with 8 electrons. On the other hand, the conduction band (CB) is dominated by Y 4d states, yttrium being an early transition element of the 2nd period. This can be quantified from the relative position versus E_F of the *n*d band middles defined by the Hankel spherical waves in ASW formalism. For Ni and Y d bands versus the Fermi level, we have: $E_{\text{Hankel}}(\text{Ni}) = 0.83$ eV < E_F = 1 eV < $E_{\text{Hankel}}(\text{Y}) = 1.42$ eV; i.e. a centering of Ni (3d) below E_F and Y (4d) above E_F. Nevertheless itinerant states arising from yttrium 4d are found within the VB; they ensure for the chemical bonding with the valence states of Ni.

For the hydrides, the similar peak shapes observed through the VB indicates a quantum mixing between the constituents. A visual inspection of the three PDOS plots shows a narrowing for both Ni and Y energy intervals within the VB proportional to the amount of H within the structure. This is accompanied with more localized and intense peaks, especially for nickel. These are the respective consequences of the volume increase leading to larger inter atomic separations and of the extra electrons brought by additional hydrogen.

The novel feature of the PDOS for the hydrides (Fig. 3b and c) with respect to YNi is the emergence of extra states created in the lower part of the VB, i.e. between −4 and −10 eV. These become more extended and broadened. Also, a sharp PDOS peak below E_F and at −6 eV is noticed for the hydrides. This peak becomes increasingly localized upon going from the tri- to the tetra-hydride. Such a feature is due to a development of out-of-plane Ni orbitals, e.g. d_{yz} orbitals which ensure for σ and σ^* bonding with H at −6 and −1 eV, respectively.

4.2. Chemical bonding

The chemical bonding is qualitatively discussed based on the integrated unit-less COOP (*i*COOP). The plots for metal-H interactions within both hydrides are shown in Fig. 4. Hydrogen occupancy ratio is respected, meaning that twice more H2 are accounted for. Major bonding comes from Ni–H interactions due to their shorter separations with respect to Y–H (cf. Table 1). For $YNiH_3$, although there are twice more H2 atoms with shorter Ni–H2 separations with respect to Ni–H1, the *i*COOP surfaces Ni–H2 are not twice as large as Ni–H1. This feature can be related to the atomic surroundings for H: [Y_3Ni_2] trigonal bipyramids for

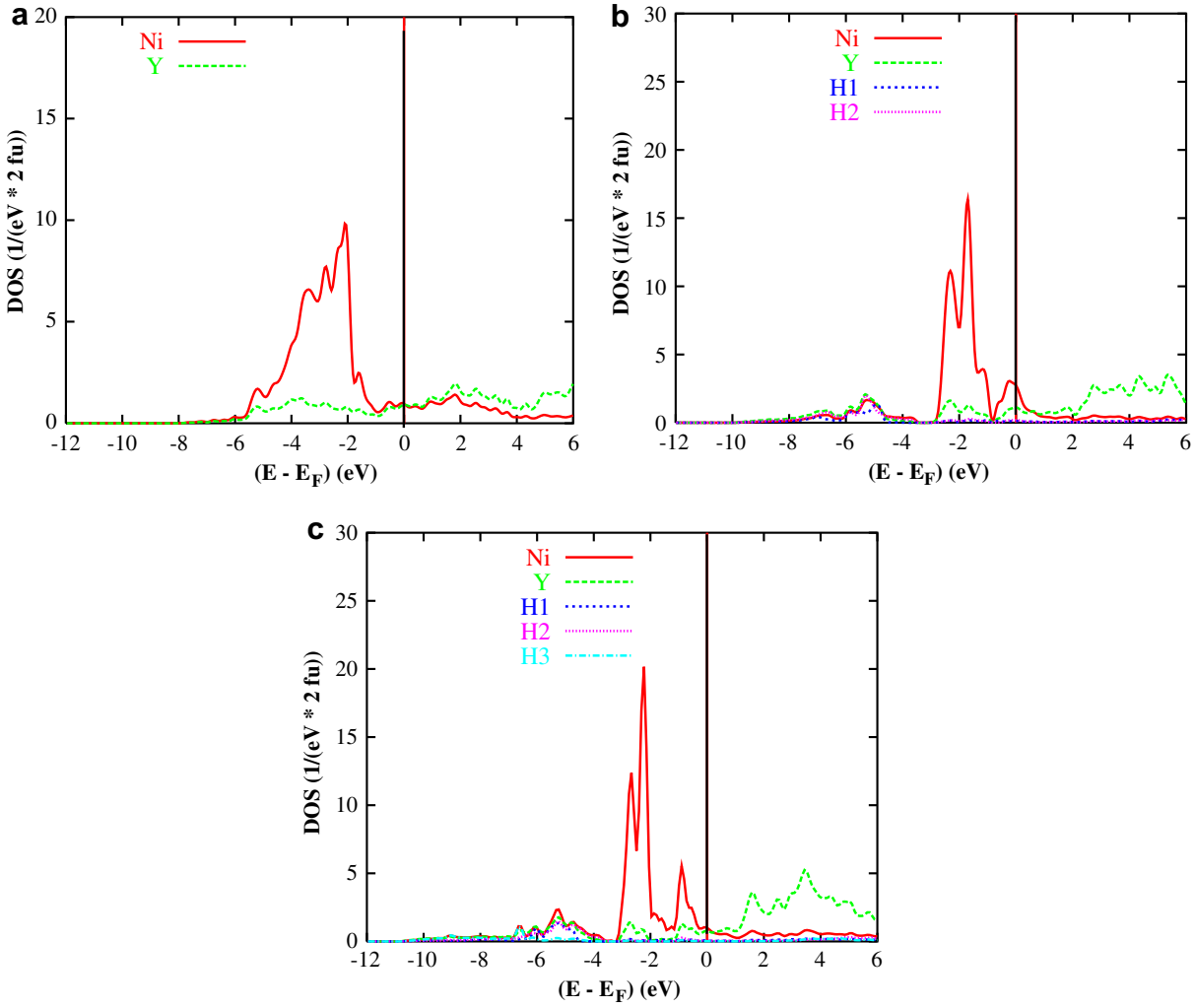

Fig. 3. Site projected density of states for (a) CrB-type YNi, (b) $YNiH_3$ and (c) $YNiH_4$.

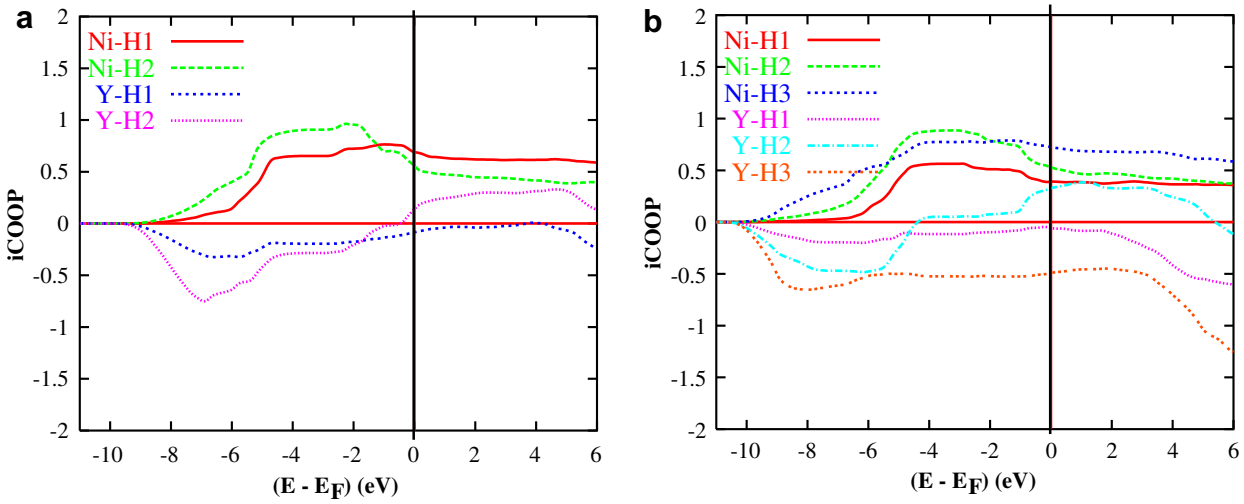

Fig. 4. Integrated COOP (*i*COOP, unit-less) for metal–hydrogen interactions in (a) $YNiH_3$ and (b) $YNiH_4$.

H1 and [Y_3Ni] tetrahedra for H2 (cf. Fig. 2), indicating twice more Ni nearest neighbors for H1. Y–H bonding is however present although with an overall low and anti-bonding like intensity.

Turning to the tetra-hydride, the same general features apply with however a major difference of a weaker overall Ni–H bonding, especially for H3 whose interaction character is weakly bonding

and strongly anti-bonding with Ni and Y, respectively. Then this would explain the smaller magnitude of the binding of hydrogen upon going from the tri- to the tetra-hydride and its enhanced covalent character.

5. Conclusion

The aim of this work based on properties obtained from DFT electronic structure methods, was to address the ground state of YNi intermetallic and the changes brought by the insertion of hydrogen leading to experimentally observed $YNiH_3$ and $YNiH_4$.

In view of experimental controversial assessments on the ground state crystal structure of YNi, we firstly established the corresponding equations of states for YNi in the proposed crystal structures in literature. From small energy differences we confirm the orthorhombic FeB-type structure as the ground state one. We also noted that the CrB-type structure adopted by the hydrides is the least stable one. Geometry optimization leads to position hydrogen within the hydride lattice. Also it is suggested that H is less stabilized in the tetra-hydride with a small covalent charge characterizing it leading to suggest it as first desorbing species among the three crystallographically different hydrogen atoms. The analyses of the DOS and chemical bonding point to large changes within the valence band with new states brought by hydrogen and a larger localization of Y and Ni partial DOS. The overall Ni–H bonding is found larger versus Y–H. Further, its differentiation for the respective H sublattices is argued based on the coordination polyhedra.

Acknowledgments

Computational facilities were provided by the University Bordeaux 1, MCIA.

References

[1] X. Huang, G.J. Ackland, K.M. Rabe, Nat. Mater. 2 (2003) 307.
[2] H. Zahres, M. Acet, W. Stamm, E.F. Wassermann, J. Alloys Compd. 72 (1988) 80.
[3] J.-L. Bobet, E. Grigorova, B. Chevalier, M. Khrussanova, P. Peshev, Intermetallics 14 (2006) 208.
[4] W.L. Korst, Acta Cryst. 66 (1962) 370;
M.E. Kirkpatrick, D.M. Bailey, J.F. Smith, Acta. Cryst. 15 (1962) 252.
[5] Y.L. Yaropolov, B.N. Verbetsky, V.A. Somenkov, in: Proceeding of Hydrogen Materials Science and Chemistry of Carbon Nanomaterials ÏCHMS'2009", pp. 192–193.
[6] J.J. Reilly, R.H. Wiswall Jr., Inorg. Chem. 7 (1968) 2254.
[7] J.F. Smith, D.A. Hansen, Acta Cryst. 18 (1965) 60.
[8] K. Klepp, E. Parthé, Acta Cryst. B 36 (1980) 3093.
[9] M. Nakhl, B. Chevalier, J.-L. Bobet, B. Darriet, J. Alloys Compd. 299 (2000) 94.
[10] P. Hohenberg, W. Kohn, Phys. Rev. 136 (1964) 864.
[11] W. Kohn, L.J. Sham, Phys. Rev. 140 (1965) 1133.
[12] A.F. Al Alam, S.F. Matar, N. Ouaini, M. Nakhl, Eur. Phys. J. B 65 (2008) 491.
[13] G. Kresse, J. Furthmüller, Phys. Rev. B 54 (1996) 11169.
[14] S.F. Matar, Progress in Solid State Chem, Intermetallic Hydrides: A Review With ab initio Aspects, (in press), doi:10.1016/j.progsolidstchem.2010.08.003.
[15] D.M. Ceperley, B.J. Alder, Phys. Rev. Lett 45 (1980) 1196.
[16] J. Perdew, K. Burke, M. Ernzerhof, Phys. Rev. Lett. 77 (1996) 3865.
[17] V.I. Anisimov, J. Zaanen, O.K. Anderson, Phys. Rev. B 44 (1991) 943.
[18] P.E. Blöchl, Phys. Rev. B 50 (1994) 17953.
[19] G. Kresse, J. Joubert, Phys. Rev. B 59 (1999) 1758.
[20] M. Methfessel, A.T. Paxton, Phys. Rev. B 40 (1989) 3616.
[21] W. Tang, E. Sanville, G. Henkelman, J. Phys.: Condens. Matter. 21 (2009) 084204. And a web ref. http://www.chemistry.mcmaster.ca/aim/aim_0.html.
[22] A.R. Williams, J. Kübler, C.D. Gelatt, Phys. Rev. B 19 (1979) 6094.
[23] V. Eyert, The Augmented Spherical Wave Method – A Comprehensive Treatment, Lect. Notes Phys., vol. 719, Springer, Berlin Heidelberg, 2007.
[24] Z. Wu, R.E. Cohen, Phys. Rev. B 73 (2006) 235116.
[25] V. Eyert, K.-H. Höck, Phys. Rev. B 57 (1998) 12727.
[26] R. Hoffmann, Angew. Chem. Int. Ed. Engl. 26 (1987) 846.
[27] S.F. Matar, V. Eyert, CNRS internal report, 1995 (unpublished).
[28] R. Dronskowski, P.E. Blöchl, J. Phys. Chem. 97 (1993) 8617.
[29] G. Bester, M. Fähnle, J. Phys: Condens. Matter. 13 (2001) 11541.
[30] F. Birch, J. Geophys. Res. 83 (1978) 1257.
[31] S.F. Matar, Solid State Sci. 12 (2010) 59.
[32] S.W. Peterson, V.N. Sadana, W.L. Korst, J. de Physique (Paris) 25 (1964) 451.
[33] S.F. Matar, Chem. Phys. Lett. 473 (2009) 61.
[34] L. Pauling, Nature of the Chemical Bond, 3rd ed., Cornell University Press, Ithaca, NY, 1960. pp. 88–107.